Loughborough University

This item was submitted to Loughborough's Research Repository by the author.
Items in Figshare are protected by copyright, with all rights reserved, unless otherwise indicated.

A combined analytical-experimental investigation of friction in cylinder liner inserts under mixed and boundary regimes of lubrication

PLEASE CITE THE PUBLISHED VERSION

http://dx.doi.org/10.1002/ls.1369

PUBLISHER

© The Authors. Published by John Wiley & Sons Ltd.

VERSION

VoR (Version of Record)

PUBLISHER STATEMENT

This work is made available according to the conditions of the Creative Commons Attribution 4.0 International (CC BY 4.0) licence. Full details of this licence are available at: http://creativecommons.org/licenses/by/4.0/

LICENCE

CC BY 4.0

REPOSITORY RECORD

Gore, Michael, Nick Morris, Ramin Rahmani, Homer Rahnejat, Paul King, and S.J. Howell-Smith. 2017. “A Combined Analytical-experimental Investigation of Friction in Cylinder Liner Inserts Under Mixed and Boundary Regimes of Lubrication”. Loughborough University. https://hdl.handle.net/2134/23880.

LUBRICATION SCIENCE
Lubrication Science 2017; **29**:293–316
Published online 16 January 2017 in Wiley Online Library (wileyonlinelibrary.com). DOI: 10.1002/ls.1369

A combined analytical-experimental investigation of friction in cylinder liner inserts under mixed and boundary regimes of lubrication

M. Gore[1], N. Morris[2], R. Rahmani[2,*,†], H. Rahnejat[2], P. D. King[2] and S. Howell-Smith[3]

[1]*Red Arch Manufacturing Ltd, Daventry, Northamptonshire, UK*
[2]*Wolfson School of Mechanical, Electrical and Manufacturing Engineering, Loughborough University, Loughborough, UK*
[3]*Capricorn Automotive Ltd, Basingstoke, Hampshire, UK*

ABSTRACT

It is necessary to develop an analytical solution in order to combine predictions with measured tribological parameters and fundamentally understand the mechanism of lubrication in a typical region of engine cycle, using tribometric studies. This paper deals with the development of such a representative approach. An analytical, rather than a numerical approach is expounded, as it is shown to suffice for the purpose of precise time-efficient predictions, which conform well to the measurements. The effect of surface topography, material and operating conditions are ascertained for the representative case of top compression ring—cylinder liner contact at the top dead centre reversal in transition from the compression to power stroke. Stainless steel uncoated surface used as press fit cylinder liners for niche original equipment manufacturer applications are compared with those furnished with a Nickel-Silicon Carbide wear-resistant coating of choice in high performance motorsport. © 2017 The Authors *Lubrication Science* Published by John Wiley & Sons Ltd.

Received 12 April 2016; Revised 31 August 2016; Accepted 27 November 2016

KEYWORDS: sliding tribometer; floating plate; boundary friction; viscous shear; Ni-SiC coating; asperity interactions

NOMENCLATURE

A	contact area
A_a	asperity contact area
b	ring (strip) contact face-width
c	location of lubricant film rupture (cavitation zone boundary)

*Correspondence to: R. Rahmani, Wolfson School of Mechanical and Manufacturing Engineering, Loughborough University, Loughborough, UK.
†E-mail: R.Rahmani@lboro.ac.uk

© 2017 The Authors *Lubrication Science* Published by John Wiley & Sons Ltd.
This is an open access article under the terms of the Creative Commons Attribution License, which permits use, distribution and reproduction in any medium, provided the original work is properly cited.

E	Young's modulus of elasticity
E'	composite (equivalent) Young's modulus of elasticity
E^*	reduced Young's modulus of elasticity
F	applied contact load
$F_{5/2}$, F_2	statistical functions
f	total friction
f_b	boundary friction
f_v	viscous friction
h	film shape
h_0	minimum film thickness
h_c	critical film thickness
h_{rc}	ring (strip) crown height
h_s	ring (strip) face profile
L	ring length in the lateral direction
l_c	critical length
M, N	intermediate variables
p	pressure
R	radius of curvature of the ring (strip) contact face
s	arbitrary integration variable
t	time
U	sliding velocity
W	total load carrying capacity
W_a	load carried by the asperities
W_h	hydrodynamic reaction
$W_h^{`}$	hydrodynamic load carrying capacity per unit lateral width
x, y	Cartesian coordinates

GREEK SYMBOLS

δ	localised Hertzian deformation
ξ	number of asperity peaks per unit area
κ	average asperity tip radius
σ	composite standard deviation of surface roughness
λ	Stribeck lubricant film ratio
λ_c	critical film ratio
ε	error of convergence for load balance
φ^*	standard height distribution
ψ	numerical damping factor
η	lubricant dynamic viscosity
υ	Poisson's ratio
τ_0	Eyring shear stress
τ_v	viscous shear
ς	coefficient of boundary shear strength of asperities

© 2017 The Authors *Lubrication Science* Published by John Wiley & Sons Ltd.
DOI: 10.1002/ls

SUPERSCRIPTS

n iteration step for load loop

SUBSCRIPTS

1,2 denotes property of plate or strip
S, N denotes property of steel or Ni-SiC surface

ABBREVIATIONS

Ni-SiC nickel silicon carbide
TDC top dead centre

INTRODUCTION

Reciprocating sliding contacts, such as the piston-cylinder system are often subject to a broad range of regimes of lubrication, from boundary to hydrodynamics. Under boundary and mixed regimes of lubrication, frictional losses of piston and ring-pack conjunctions can account for a significant proportion of the overall frictional losses from an IC engine.[1] Of the components in this system, the share of frictional losses of the top compression ring is one of the largest,[2] because of its close adherence to the cylinder liner surface to seal the combustion chamber from the bottom end of the engine. Considering its usual small contact area (circa 300 mm^2), it contributes up to 3% of total fuel energy consumption in a typical automotive engine.[3,4] Therefore, understanding and subsequent palliation of these losses has attracted considerable attention. The transient nature of the compression ring-cylinder liner contact and the broad range of cyclic regimes of lubrication make the nature of analysis quite complex.[5]

There are a host of influential parameters, often interacting in a non-linear fashion. These include the effect of ring contact face geometry and topography,[6–8] which are also subject to wear.[9–11] Owing to the variations in the applied gas pressure, the ring is subject to elastic modal behaviour both in its radial plane as well as out of plane motion in twist and bending.[12,13] Additionally, the heat generated due to combustion as well as shear of the lubricant film and any direct boundary interaction also affects the tribological conditions.[14–16] The complexity of the problem is exacerbated by ring-bore conformability[17,18] and particularly with realistic out-of-roundness of the bore taken into account.[19] Furthermore, the lubricant flow into the contact conjunction is far more complex than an assumed flooded inlet on the account of reverse and recirculating flow, starvation,[20] cavitation and lubricant film reformation at the contact exit.[20–22] Therefore, complex boundary conditions exist in practice,[23] which are often not taken into account in predictive analyses.

As a result of the complexities of the multi-variate and interactive nature of the problem, tribometric studies have received much attention in recent years in order to gain a fundamental understanding of the effect of some of the aforementioned parameters in isolation from the others. The sliding tribometers have been extensively used. Dearlove and Cheng[24] and Ting[25] designed a slider test rig

© 2017 The Authors *Lubrication Science* Published by John Wiley & Sons Ltd.
DOI: 10.1002/ls

by converting a conventional piston-cylinder system to study the tribology of ring-bore friction under motored conditions. The former measured both friction and film thickness; whilst the latter only measured the contact friction. Dearlove and Cheng[24] measured friction using a load cell which was mounted onto a floating liner sample. The film thickness was measured using the laser-induced florescence technique. Akalin and Newaz[26] and Bolander et al[27] also developed slider rigs based on motored engine cylinders, measuring friction under mixed regime of lubrication. The former used a strain gauge system to measure friction, whilst the latter measured film thickness, using fibre-optic displacement sensors, mounted onto a pivot arm. For measurement of friction, Furuhama and Sasaki[28] were amongst the first to propose the use of a floating liner. The technique was improved by Gore et al[29] using precision piezoelectric load cells intervening between the floating liner and the cylinder block, with gas pressure contained within the chamber using a labyrinth seal. In this manner, friction was measured directly under fired engine conditions in a single cylinder high performance engine.

With motored cylinder systems, described earlier, there is still a fair number of parametric interactions. To reduce these effects to basic study of surface materials (including coatings), topography and lubricant types and their combinations, reciprocating plates were used by Felter et al[30] and Johansson et al,[31] where the plate was made of cylinder liner material and a stationary loaded block, representing the counter face surface. They measured friction using a transducer mounted onto the block. Truhan et al[32] also studied the effect of lubrication conditions on the frictional and wear behaviour of ring-liner contact using a Cameron-Plint high frequency reciprocating test rig with different coated surfaces. Sliding tribometers have also been used to study the effect of surface texturing,[33] surface scuffing,[34] as well as observation of cavitation.[35]

In the current study, a precision sliding tribometer is used to study frictional performance of a series of coated plates used as cylinder liner material, particularly for advanced high-performance engines.

Cylinder liners used in the IC engines are usually made of cast iron, steel or high grade aluminium for some high performance race engines. Progressively, use of hard wear-resistant coatings for cylinder liner, top compression ring contact face or both, particularly in niche original equipment manufacturer and racing applications has been adopted. Styles et al[11] described the use of plasma sprayed Ni-chromium nitride coating with inclusion of molybdenum to reduce the solid solubility of the coating with a standard cast iron liner. Plasma sprayed coating is porous, thus aiding retention of lubricant. Tung and Gao[36] studied friction and wear performance of thermal-sprayed chromium nitride and physical vapour deposited diamond-like carbon on nitrided stainless steel and chrome-plated stainless steel piston rings. Nickel silicon carbide (Ni-SiC) is the coating of choice for cylinder liners in motorsport applications. Howell-Smith et al[37] used a number of coated cylinder liners, including Ni-SiC as well as plasma-assisted physical vapour deposited diamond-like carbon coating. These were subjected to accelerated wear under fired engine condition, using a motocross motorbike engine. The Ni-SiC coating on a high grade aluminium liner was shown to perform best under severe simulated cross-country race conditions. Despite a significant number of reported investigations, the fundamental question still remains with respect to the choice of cylinder coating for a broad range of applications, and particularly for the dominant mixed and boundary regimes of lubrication at the top dead centre (TDC) reversal.

The current study benchmarks the use of Ni-SiC against an uncoated steel liner for motorsport applications. A combined analytical-experimental study, using a sliding tribometer, is presented.

© 2017 The Authors *Lubrication Science* Published by John Wiley & Sons Ltd.
DOI: 10.1002/ls

TESTRIG SETUP AND EXPERIMENTAL PROCEDURE

The sliding tribometer

The in-house designed and built sliding tribometer is shown in Figure 1. The sliding head is driven through an ultra-low backlash lead-screw by an electric motor, controlled through an interface to a laptop computer, using a National Instrument data logger. The rotational speed of the lead-screw is measured by an encoder (resolution of 10 000 pulses per revolution), also interfaced to the National Instrument data logger. Two Bruel and Kjaer torsional vibrometers are used to precisely measure the torsional, as well any tilting and lateral motions of the sliding head. A proportional-integral-derivative controller for the motor speed is used to provide a reciprocal motion based on the encoder count. This arrangement is used to correct any potential errors in the measurements of the encoder or oscillatory motion caused by any backlash. A flat specimen (levelness of $\pm 0.8\mu m$) made of the same substrate material, coating and surface topography as that of a cylinder liner is mounted onto a base floating plate. This plate is mounted upon nominally frictionless bearings and is dragged by a sliding strip with the same contact face geometry as a compression ring, mounted into the loaded reciprocating head as shown in Figure 2. The strip is allowed to slightly sway; only fully constraining any rotation. This eliminates any problems associated with any waviness of the flat specimen. Loading is achieved by the application of precisely measured dead weights, which can be altered to represent loading conditions experienced by the top compression ring of a wide range of engines at the TDC reversal in transition from the compression to the power stroke ($\pm$ 10° crank-angle from the TDC), including for high-performance highly loaded engines (load per unit strip length of 400–850 $N\,m^{-1}$). This is combined with the controlled sliding speed variation in the same region, also in a range representative

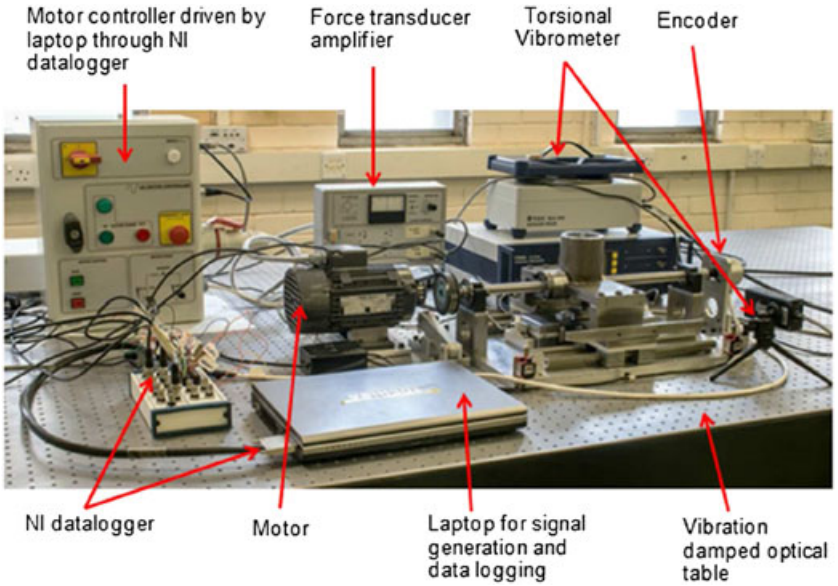


Figure 1. The precision sliding tribometer. [Colour figure can be viewed at wileyonlinelibrary.com]

© 2017 The Authors *Lubrication Science* Published by John Wiley & Sons Ltd.
DOI: 10.1002/ls

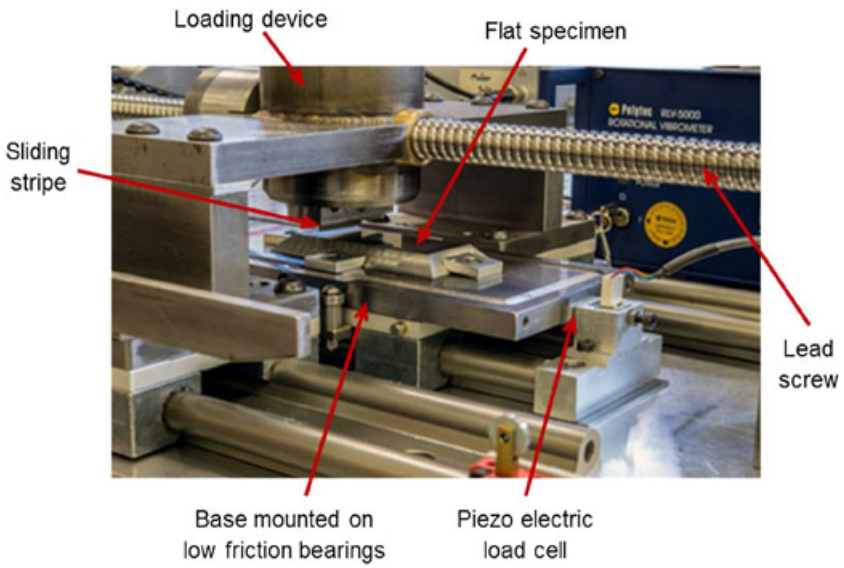


Figure 2. Detailed view of the contact in the floating plate arrangement. [Colour figure can be viewed at wileyonlinelibrary.com]

of engine conditions (circa $< \pm 0.5\ \mathrm{m\,s^{-1}}$). The tribometer is intended to replicate the conditions of the compression ring conjunction at the TDC reversal for a cold running engine, when worst tribological conditions under mixed and boundary regimes of lubrication are expected. In transition from the compression to the power stroke, a small quantity of lubricant would be expected on the free surface of the liner. Therefore, 1 mL of lubricant is applied onto the flat specimen surface and spread uniformly over it for a short period of reciprocation. This is prior to taking any measurement of friction.

The floating base plate and the mounted sample are dragged by the sliding strip through a combination of viscous friction of a formed lubricant film and any boundary interactions of the counter face opposing asperities. The surface topography of both the flat specimen sample and the sliding strip contact face are measured using infinite focus microscopy (Alicona, with measurement sensitivities of 1 *nm* in height; z and 0.18 μm in horizontal directions; x and y) prior and after testing. Two Honeywell FSG15N1A piezoelectric load cells (Figure 2) with resolution of 0.24 mV/grf were used to measure the inertial force of the dragged arrangement, ma. The force causing the inertial motion is friction, f, thus

$$\sum F = f = ma \tag{1}$$

Therefore, the tribometer forms the basis for understanding of the mechanisms of friction generation in reciprocating sliding contacts. It also provides a basis for validation of analytical/numerical techniques, which are subsequently used for prediction of friction in real engine piston systems.

© 2017 The Authors *Lubrication Science* Published by John Wiley & Sons Ltd.
DOI: 10.1002/ls

Preparation of samples

The strip and the flat specimen are lapped to a surface finish representing their counterparts in real engine applications. Figure 3 shows measurements taken from a sliding strip sample, representing a parabolic-type surface contact face-width profile.

The slider strip is initially used in a set of preliminary tests to complete the 'running-in' process. Once the surface 'peakedness' was removed, the surface topography measurements showed that the strip profile, and its topography do not alter considerably during the friction tests. Since the running time for each friction test is very short (~2.5s), this also justifies the observed insignificant change in the measured topography of run-in strip profile after each test. In addition, to avoid the occurrence of edge contact, the lateral edges of the strip were chamfered.

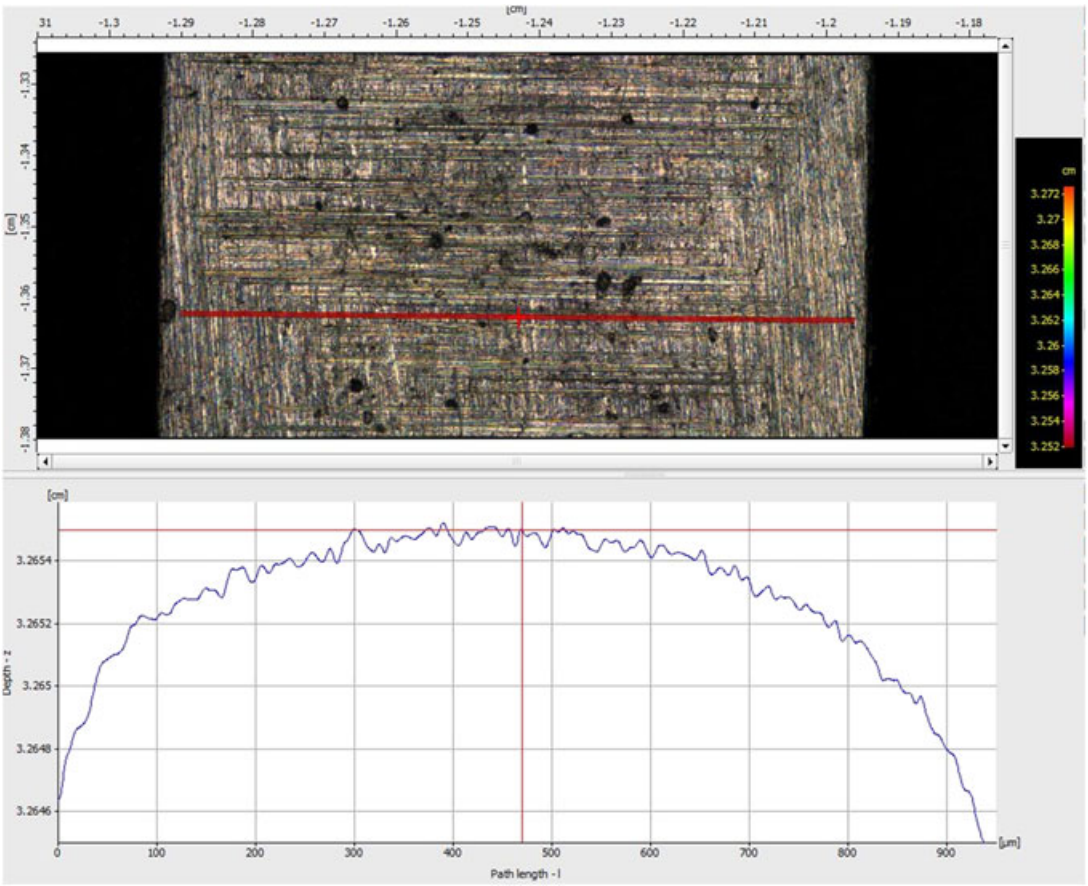


Figure 3. The parabolic profile of the sliding strip contact face through optical microscopy. [Colour figure can be viewed at wileyonlinelibrary.com]

© 2017 The Authors *Lubrication Science* Published by John Wiley & Sons Ltd.
DOI: 10.1002/ls

ANALYTICAL PREDICTIVE METHOD

Contact geometry

The profile of the sliding strip, representing that of a top compression ring in a motocross motorbike race engine with the origin of coordinate system located at the centre of face width can be described by a parabola (Figure 4):

$$h_s = \frac{1}{2R}x^2 \tag{2}$$

where, R is radius of curvature of the strip contact face-width.

Therefore, the total gap between the ring sample and specimen flat plate becomes

$$h = h_0 + \frac{1}{2R}x^2 \tag{3}$$

where, h_0 is the minimum film thickness (gap).

The ring crown height and its contact face-width radius of curvature are related as

$$\frac{h_{rc}}{(b/2)^2} = \frac{1}{2R} \tag{4}$$

in which, h_{rc} and b are the ring crown height and strip face-width, respectively.

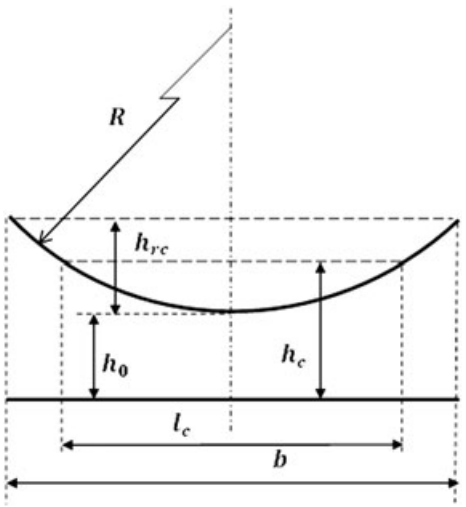


Figure 4. The schematic representation of the sliding strip and the flat specimen.

© 2017 The Authors *Lubrication Science* Published by John Wiley & Sons Ltd.
DOI: 10.1002/ls

Hydrodynamic load carrying capacity

It should be noted that for the typical applied loads on the compression ring in the vicinity of TDC reversal, no localised deformation of the ring or liner face are noted[7,18] (see Appendix). The generated pressures are also insufficient to induce any piezo-viscous action of the lubricant (i.e. iso-viscous conditions). Assuming a sliding line contact for a parabolic profile, the hydrodynamic load carrying capacity per unit lateral width for an iso-viscous lubricant under isothermal conditions become[38]

$$W_h^{'} = 2.45R\left(\frac{\eta U}{h_0}\right) \tag{5}$$

where, U is sliding velocity and η is lubricant dynamic viscosity. Equation 5 excludes the effect of squeeze film motion and assumes a fully flooded inlet with Reynolds exit boundary conditions:

$$\begin{cases} p_{x\to-\infty} = 0 \\ p_{x=c} = 0 \\ \left.\dfrac{dp}{dx}\right|_{x=c} = 0 \end{cases} \tag{6}$$

where, c is the location of lubricant film rupture; marking the start of the cavitation region, measured from geometrical centre of the strip.

For the case of the sliding strip considered here, the inlet and outlet boundary pressures at its leading and trailing edges are the atmospheric pressure (equal to gauge pressure of zero).

Equation 5 can be extended to describe the total load carrying capacity of the contact; neglecting any side leakage of lubricant from its lateral edges:

$$W_h = W_h^{'}L = 2.45LR\left(\frac{\eta U}{h_0}\right) \tag{7}$$

where, L is the length of the strip in the lateral direction.

Load carried by the asperities

The load carried by asperities is given by Greenwood and Tripp[39] as

$$W_a = \frac{16\sqrt{2}}{15}\pi(\xi\kappa\sigma)^2\sqrt{\frac{\sigma}{\kappa}}E^{'}AF_{5/2}(\lambda) \tag{8}$$

where, E' is the composite (equivalent) Young's modulus of elasticity:

$$\frac{1}{E^{'}} = \frac{1-\upsilon_1^2}{E_1} + \frac{1-\upsilon_2^2}{E_2} \tag{9}$$

and ξ, κ and σ are the number of asperity peaks in unit area, the average asperity tip radius of curvature and composite surface roughness standard deviation. In addition, $\lambda = h/\sigma$ is the Stribeck lubricant film

© 2017 The Authors *Lubrication Science* Published by John Wiley & Sons Ltd.
DOI: 10.1002/ls

ratio. $F_{5/2}$ is a statistical function of the film ratio, described by Greenwood and Tripp[39] in general form, based on the standard height distribution function $F_n(\lambda) = \int_{\lambda}^{\infty} (s-\lambda)^n \varphi^*(s) ds$, and for $n = 5/2$ is approximated by a fifth order polynomial curve-fitting in order to obtain a computationally-friendly form as[40]

$$F_{5/2}(\lambda) = \begin{cases} -0.0046\lambda^5 + 0.0574\lambda^4 - 0.2958\lambda^3 + 0.7844\lambda^2 - 1.0776\lambda + 0.6167 & ;\text{for } \lambda \le \lambda_c = 2.224 \\ 0 & ;\text{for } \lambda > \lambda_c = 2.224 \end{cases} \quad (10)$$

where, λ_c is the critical film ratio, indicating the point earlier which there would be no probability of direct asperity tip contact on the opposing surfaces.

In equation 8, A denotes the total (apparent) contact area, where the asperity tips may come into contact. Ignoring the curvature of the sliding strip face-width, the (projected) contact area may be stated as

$$A = bL \quad (11)$$

However, the ring face has a parabolic shape and the opposing asperities away from the centre of contact may never come into contact. Therefore, it is important to calculate the area of the ring face from which the film ratio falls below the critical film ratio. Considering the critical film ratio, the critical distance between the ring and plate surfaces becomes

$$h_c = \lambda_c \sigma \quad (12)$$

If the portion of the face-width whose gap with the plate surface falls below the critical film thickness is l_c, then (Figure 4)

$$h_c - h_0 = \frac{1}{2R}\left(\frac{l_c}{2}\right)^2 \quad (13)$$

Rearranging for l_c:

$$l_c = 2\sqrt{2R(h_c - h_0)} \text{ where, } h_c \ge h_0 \quad (14)$$

Therefore, the contact area in which there would be a chance of direct asperity interactions becomes

$$A = l_c L \quad (15)$$

It is important to note that since $F_{5/2}(\lambda)$ is calculated based on h_0, not all of the asperities in the contact area would contribute to the contact load carrying capacity in the same way as the

© 2017 The Authors *Lubrication Science* Published by John Wiley & Sons Ltd.
DOI: 10.1002/ls

asperities located close to the contact centre would do. Consequently, the contact area should be corrected to take this issue into account. The correction should follow the variations of $F_{5/2}(\lambda)$ with λ as shown in Figure 5.

Therefore, a more accurate representation of asperity load carrying capacity can be expressed as

$$W_a = \frac{16\sqrt{2}}{15}\pi(\xi\kappa\sigma)^2\sqrt{\frac{\sigma}{\kappa}}E'\int F_{5/2}(\lambda)dA \tag{16}$$

where, $\lambda = h/\sigma$, $h_0 \le h \le h_c$, $dA = 2Ldx$ and $0 \le x \le l_c/2$ (Figure 4).

The differentiation of the parabolic profile (equation 3) yields

$$dh = \frac{x}{R}dx = \frac{\sqrt{2Rh}}{R}dx = \sqrt{\frac{2h}{R}}dx \tag{17}$$

Therefore, dA in terms of dh becomes

$$dA = L\sqrt{\frac{2R}{h}}dh \tag{18}$$

Consequently, the integral term in W_a, can be recast as

$$\int F_{5/2}(\lambda)dA = L\sqrt{2R}\int_{h_0}^{h_c} F_{5/2}\left(\frac{h}{\sigma}\right)h^{-1/2}dh \tag{19}$$

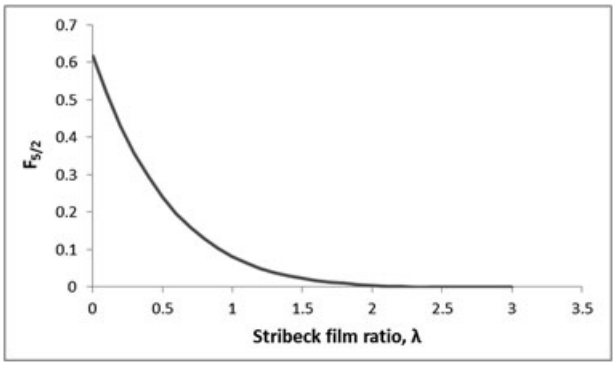


Figure 5. Variations of statistical function $F_{5/2}$ with the Stribeck lubricant film ratio, λ.

© 2017 The Authors *Lubrication Science* Published by John Wiley & Sons Ltd.
DOI: 10.1002/ls

Or in terms of λ as

$$\int F_{5/2}(\lambda)dA = L\sqrt{2\sigma R}\int_{\lambda_0}^{\lambda_c} F_{5/2}(\lambda)\lambda^{-1/2}d\lambda \tag{20}$$

where, $\lambda_0 = h_0/\sigma$ and $\lambda_c = h_c/\sigma = 2.2239$

Performing the integration, the load carried by the asperities becomes

$$W_a = \frac{16\sqrt{2}}{15}\pi(\xi\kappa\sigma)^2\sqrt{\frac{\sigma}{\kappa}}E^* L\sqrt{2\sigma R}\left\{\frac{2\sqrt{\lambda}}{3465}[\lambda(\lambda M - 1244.628) + 2136.8655]\right\}_{\lambda_0}^{\lambda_c} \tag{21}$$

where, $M = -1.449\lambda^3 + 22.099\lambda^2 - 146.421\lambda + 543.5892$.

Since in the mixed regime of lubrication the applied load is carried by the hydrodynamic reaction as well as asperity interactions, then

$$W = W_h + W_a \tag{23}$$

The iterative procedure for the analytical study assumes an initial gap of h_0. Then, the earlier components of total contact load are obtained.

At each time step during simulation, a quasi-static balance is sought as

$$\frac{|F - W|}{F} < \varepsilon \cong 10^{-3} \tag{24}$$

If the earlier convergence criterion is not met, then the assumed value of h_o is corrected as

$$h_0^n = h_0^{n-1}\left[1 + \psi\left(\frac{W - F}{F}\right)\right] \tag{25}$$

where, ψ is found empirically and set as high as possible in order to achieve rapid convergence, whilst maintaining numerical stability. A typical value of $\psi \cong 0.075$ is obtained. Once convergence is obtained the simulation is advanced to the next time step.

Friction

The total generated contact friction between the sliding strip and the flat specimen is as the result of viscous shear of a lubricant film as well as the interaction of opposing asperities on the contiguous surfaces:

$$f = f_v + f_b \tag{26}$$

The viscous shear stress is given as

$$\tau_v = \frac{\eta U}{h_0} \tag{27}$$

© 2017 The Authors *Lubrication Science* Published by John Wiley & Sons Ltd.
DOI: 10.1002/ls

This is the shear stress caused by Couette flow of the lubricant drawn into the conjunction by the relative sliding motion of the strip with respect to the flat specimen surface. In the current study, the Poiseuille component of shear, induced by the pressure gradient at the inlet conjunction, is ignored as the pressure gradient is deemed quite low for thin films and low pressure conjunctions, particularly under mixed and boundary regimes of lubrication.

Hence, viscous friction becomes

$$f_v = \tau_v A = \frac{\eta U}{h_0} bL \tag{28}$$

However, due to the curvature of the ring face, the equation needs to be modified to

$$f_v = L\int_0^b \frac{\eta U}{h(x)} dx = \eta UL \int_{-b/2}^{b/2} \frac{1}{h(x)} dx \tag{29}$$

and for the parabolic ring profile, it can be recast as

$$f_v = 2\eta UL \int_0^{b/2} \frac{1}{h(x)} dx = 2\eta UL \sqrt{\frac{2R}{h_0}} \tan^{-1}\left(\frac{b}{2\sqrt{2Rh_0}}\right) \tag{30}$$

The boundary friction is calculated using[11,41]

$$f_b = \tau_0 A_a + \varsigma W_a \tag{31}$$

where, τ_0 is the Eyring shear stress, ς stands for the pressure coefficient of boundary shear strength of the softer of the two interfaces. The value of this parameter is usually obtained using an atomic force microscope in lateral force mode.[11] The same procedure as in[11] is carried out, obtaining appropriate values for all of the specimens used in this study (Table I). A_a represents the total contact area of the asperity tips on the opposing surfaces[39]:

$$A_a = \pi^2 (\xi \kappa \sigma)^2 A F_2(\lambda) \tag{32}$$

where, F_2 is a statistical function (with the generic form F_n with $n=2$ as described earlier) of the Stribeck lubricant film ratio, which is approximated by a fifth order polynomial[40]:

$$F_2(\lambda) = \begin{cases} -0.0018\lambda^5 + 0.0281\lambda^4 - 0.1728\lambda^3 + 0.5258\lambda^2 - 0.8043\lambda + 0.5003 & ;\text{for } \lambda \leq \lambda_c = 2.295 \\ 0 & ;\text{for } \lambda > \lambda_c = 2.295 \end{cases} \tag{33}$$

Figure 6 shows the variation of this function with the lubricant film ratio.

© 2017 The Authors *Lubrication Science* Published by John Wiley & Sons Ltd.
DOI: 10.1002/ls

Table I. Input data for the two studied cases.

Parameter	Case I (with steel plate)	Case II (with Ni-SiC coated plate)	Unit
Strip material	Stainless steel 440C	Stainless steel 440C	—
Plate material	Steel	Steel with Ni-SiC coating	—
Strip material modulus of elasticity	200	200	GPa
Plate (coating) material modulus of elasticity	203	160	GPa
Strip material Poisson ratio	0.3	0.3	—
Plate (coating) material Poisson ratio	0.3	0.23	—
Strip contact face-width	1.0	1.0	mm
Strip lateral length	30	30	mm
Strip face radius of curvature	31	31	mm
Composite standard deviation of surface roughness	0.126	0.346	mm
Roughness parameter $\xi\kappa\sigma$	0.659	1.56	—
Roughness slope σ/κ	3.05e−5	1.20e−4	—
Pressure coefficient of boundary shear strength for the plate material	0.22	0.26	—
Eyring shear stress	2.0	2.0	MPa
Lubricant density (@15°C)	833.0	833.0	$kg\,m^{-3}$
Lubricant dynamic viscosity (@20°C)	0.17	0.17	Pa.s
Applied normal load on the strip	11.0	11.0	N

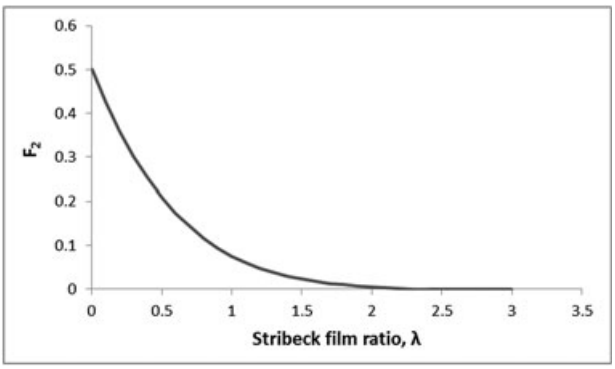


Figure 6. Variations of statistical function F_2 with Stribeck film ratio, λ.

The total contact area is obtained as before, thus

$$A_a = \pi^2(\xi\kappa\sigma)^2 \int F_2(\lambda) dA \tag{34}$$

where, $\lambda = h/\sigma$, $h_0 \le h \le h_c$, $dA = 2Ldx$ and $0 \le x \le l_c/2$ (Figure 4).

© 2017 The Authors *Lubrication Science* Published by John Wiley & Sons Ltd.
DOI: 10.1002/ls

With a parabolic profile, the integral term in A_a becomes

$$\int F_2(\lambda)dA = L\sqrt{2\sigma R}\int_{\lambda_0}^{\lambda_c} F_2(\lambda)\lambda^{-1/2}d\lambda \tag{35}$$

where, $\lambda_0 = h_0/\sigma$ and $\lambda_c = h_c/\sigma = 2.2239$.

Performing the integration, the asperity contact area can be recast as

$$A_a = \pi^2(\xi\kappa\sigma)^2 L\sqrt{2\sigma R}\left\{\frac{2\sqrt{\lambda}}{3465}[\lambda(\lambda N - 928.9665) + 1733.5395]\right\}_{\lambda_0}^{\lambda_c} \tag{36}$$

where, $N = -0.567\lambda^3 + 10.8185\lambda^2 - 85.536\lambda + 364.3794$.

Consequently boundary friction becomes

$$\begin{aligned} f_b = {} & \tau_0\pi^2(\xi\kappa\sigma)^2 L\sqrt{2\sigma R}\left\{\frac{2\sqrt{\lambda}}{3465}[\lambda(\lambda N - 928.9665) + 1733.5395]\right\}_{\lambda_0}^{\lambda_c} + \\ & \varsigma\frac{16\sqrt{2}}{15}\pi(\xi\kappa\sigma)^2\sqrt{\frac{\sigma}{\kappa}}E^* L\sqrt{2\sigma R}\left\{\frac{2\sqrt{\lambda}}{3465}[\lambda(\lambda M - 1244.628) + 2136.8655]\right\}_{\lambda_0}^{\lambda_c} \end{aligned} \tag{37}$$

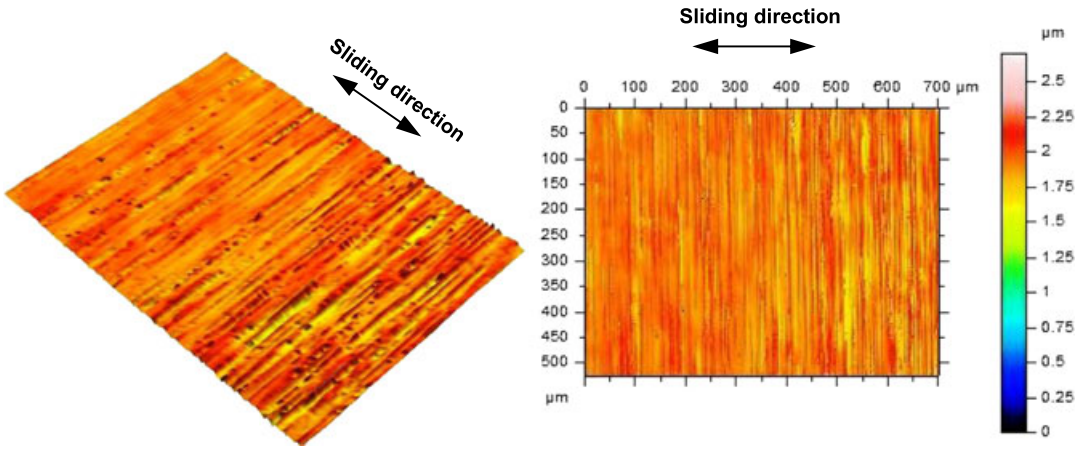
Finally, the total generated friction is obtained by substitution of f_b in equation 26, thus

$$\begin{aligned} f = {} & 2\eta UL\sqrt{\frac{2R}{h_0}}\tan^{-1}\left(\frac{b}{2\sqrt{2Rh_0}}\right) + \tau_0\pi^2(\xi\kappa\sigma)^2 L\sqrt{2\sigma R}\left\{\frac{2\sqrt{\lambda}}{3465}[\lambda(\lambda N - 928.9665) + 1733.5395]\right\}_{\lambda_0}^{\lambda_c} + \\ & \varsigma\frac{16\sqrt{2}}{15}\pi(\xi\kappa\sigma)^2\sqrt{\frac{\sigma}{\kappa}}E^* L\sqrt{2\sigma R}\left\{\frac{2\sqrt{\lambda}}{3465}[\lambda(\lambda M - 1244.628) + 2136.8655]\right\}_{\lambda_0}^{\lambda_c} \end{aligned} \tag{38}$$

MEASURED INPUT DATA FOR THE ANALYSIS

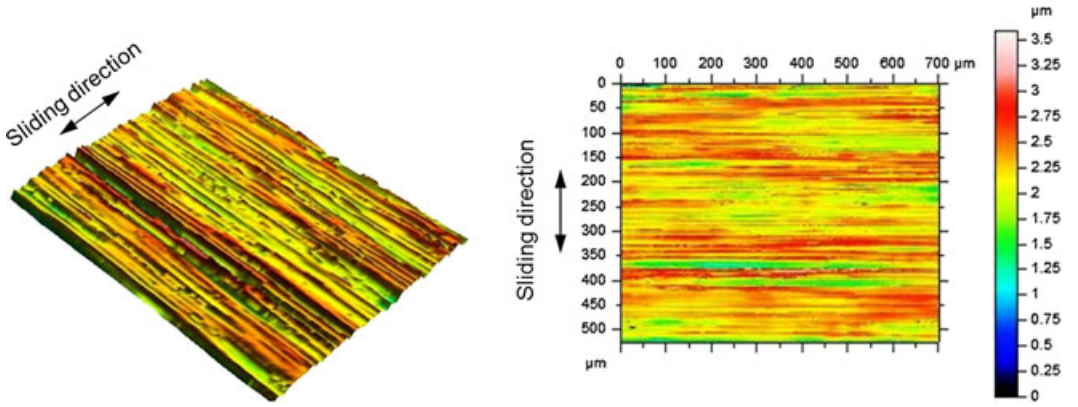
Two specimens representing the material of choice for many cylinder liners are used. One specimen is an uncoated steel, often used as a thin press fit liner into niche original equipment manufacturer engines. The other is the same steel substrate material, coated with an approximately 20 μm of Ni-SiC. This is the coating of choice for most motorsport applications. Both flat test pieces were ground on a centre-less grinder and honed. Note that a rougher surface resulted by centre-less grinding of the Ni-SiC coated surface. This is because Ni-SiC is a hard, wear-resistant coating compared with the uncoated steel specimen, which is more ductile and malleable. Figures 7 and 8 show optical microscopy images of the steel and Ni-SiC flat plates, respectively. These are obtained by an Alicona infinite focus microscope with a nominal vertical resolution of 1 *nm* and lateral resolution of 0.18 μm in the lateral

© 2017 The Authors *Lubrication Science* Published by John Wiley & Sons Ltd.
DOI: 10.1002/ls



(a) (b)

Figure 7. (a) 3D and (b) 2D view of the measured steel plate surface. [Colour figure can be viewed at wileyonlinelibrary.com]



(a) (b)

Figure 8. (a) 3D and (b) 2D view of the measured Ni-SiC plate surface. [Colour figure can be viewed at wileyonlinelibrary.com]

horizontal directions. A Large number of scanned areas were used to obtain average values for all topographical parameters established. A relevant set of surface roughness statistical parameters, asperity distribution and geometry are obtained from post processing of the optical images and are listed in Table I, together with other required data as input for the analytical simulations.

© 2017 The Authors *Lubrication Science* Published by John Wiley & Sons Ltd.
DOI: 10.1002/ls

In order to ensure repeatability of testing conditions, a base lubricant without boundary active species is used. Formulated lubricants contain boundary active lubricant species such as friction modifiers, surfactants and other constituents, which may adsorb or chemically bond to the contacting surfaces, and are quite difficult to remove. As a result, repeatability of testing would be difficult. Therefore, the base oil, which underlies the usual lubricant SAE 10W40, is used. The rheological data is listed in Table I.

RESULTS AND DISCUSSION

Experimental results

The speed of sliding is kept quite low, representative of TDC reversal. This also encourages mixed or boundary regimes of lubrication. The speed of the rotation of the reciprocating lead-screw is monitored by an encoder and converted to the sliding speed through pitch of the lead-screw. The variation is shown in Figure 9.

After an initial accelerative phase, the speed of sliding is kept constant as far as possible. The 'noise' resident on the measured signal is as the result of a combination of causes. One is the vibration of the driving motor, the other is the stick-slipping of the toothed belt drive system, another is some degree of backlash oscillations of the lead-screw at low speed operation, and finally there is some effect from contact stick-slip motion. Some of these are attenuated through application of belt tension control and use of a high ultra-precision lead-screw.

Figure 10 shows the measured friction trace, corresponding to the sliding motion in Figure 9.

With an applied contact load of 11N, the variations in the coefficient of friction are shown in Figure 11. This shows an average value for coefficient of friction of $\mu = 0.225$, indicating that a mixed to boundary regime of lubrication is prevalent. Note that for fluid film regime of lubrication, one would expect a value in the range 0.005–0.05.

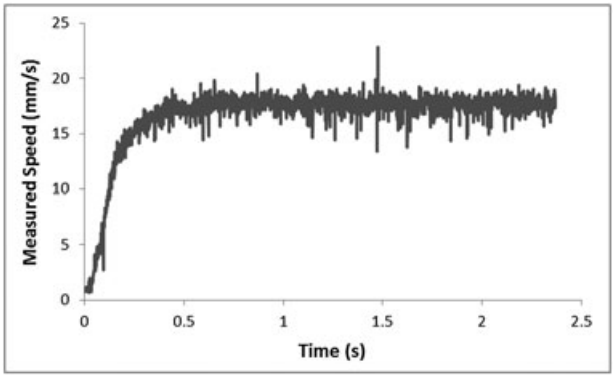


Figure 9. The measured sliding speed of the slider.

© 2017 The Authors *Lubrication Science* Published by John Wiley & Sons Ltd.
DOI: 10.1002/ls

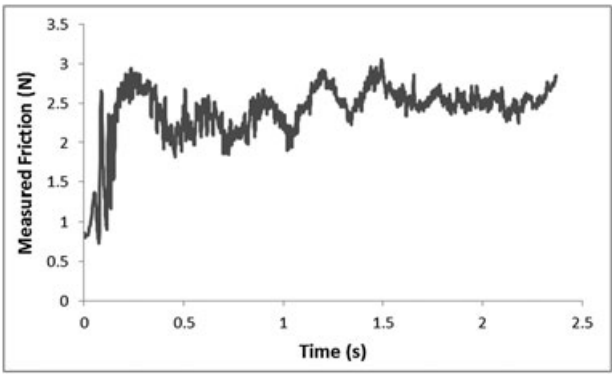


Figure 10. Measured sliding friction for the case of Ni-SiC coated plate.

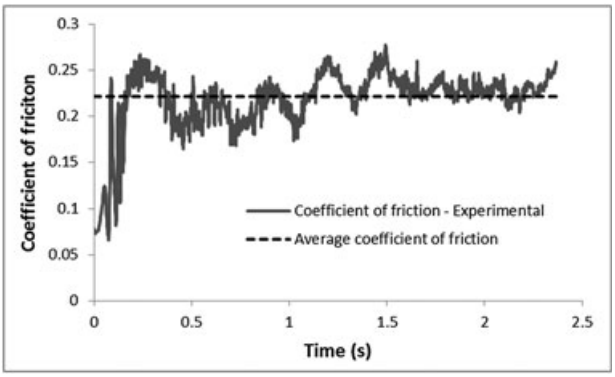


Figure 11. Measured coefficient of friction for the steel ring strip sliding on the Ni-SiC coated flat specimen.

Numerical predictions and comparison with measurements

It is possible to use the measured sliding speed and the analytical method expounded earlier to show the variations in the minimum film thickness for the two cases of coated and uncoated plates. This is shown in Figure 12. It can be seen that a very thin film is predicted in both cases. Aside from the initial accelerative phase, a fairly consistent film is predicted with slightly higher thickness for the case of Ni-SiC coated substrate.

The regime of lubrication can be ascertained by plotting the predictions in the form of the Stribeck lubricant film parameter. This is shown in Figure 13. Note that the critical value of this parameter, $\lambda_c = 2.3$, after which mixed or boundary regimes of lubrication are encountered. This critical value is also shown in Figure 13. Since the uncoated steel plate has a superior honed surface post centre-less grinding, it is clear that the Stribeck parameter remains above the indicated critical value. This means that a hydrodynamic regime of lubrication should be prevalent. For the case of Ni-SiC coating, the Stribeck parameter remains close to its critical value, thus; a mixed regime of lubrication is expected.

© 2017 The Authors *Lubrication Science* Published by John Wiley & Sons Ltd.
DOI: 10.1002/ls

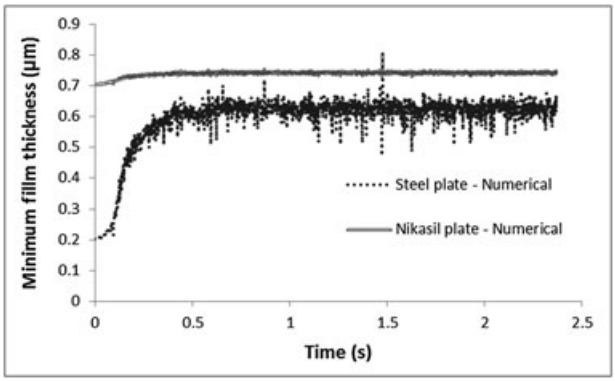


Figure 12. Minimum film thickness variation for uncoated and coated contact during the prescribed sliding motion.

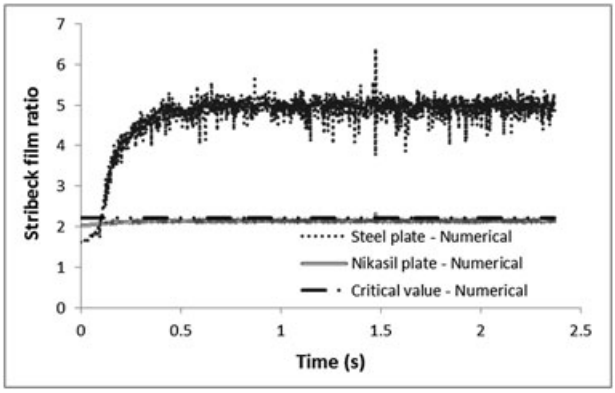


Figure 13. Determined regime of lubrication for the cases studied.

The predicted load carrying capacity should equate the applied load. If the predictions in Figure 13 were to be upheld, then the contributions to the load carrying capacity from boundary and viscous friction should show that in the case of steel plate the contribution is entirely due to hydrodynamic pressures. In the case of Ni-SiC coating, there must be a significant portion of predicted load carried by the asperities. Figures 14 and 15 below confirm this supposition.

In the case of the steel plate, the entire load is supported by the hydrodynamic reaction; whereas in the case of the Ni-SiC plate, a combination of hydrodynamic and boundary reactions support the carried load. Hence, a mixed regime of lubrication exists (see the asperity load shares in Figures 15). This is partly because of the rougher Ni-SiC surface, owing to the grinding process and the hard brittle nature of Ni-SiC, when compared with the uncoated steel substrate and partly because of the higher shear strength of the Ni-SiC. The repercussion is that even if nominally identical topographies could be achieved, under boundary regime of lubrication, there would be higher boundary friction with the Ni-SiC than steel. However, the wear resistance of the former is significantly superior.

© 2017 The Authors *Lubrication Science* Published by John Wiley & Sons Ltd.
DOI: 10.1002/ls

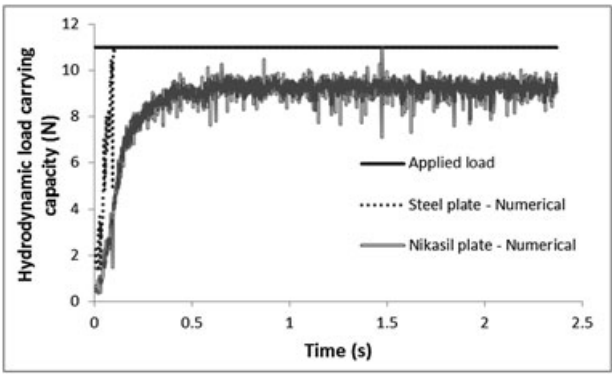


Figure 14. Predicted hydrodynamic reaction.

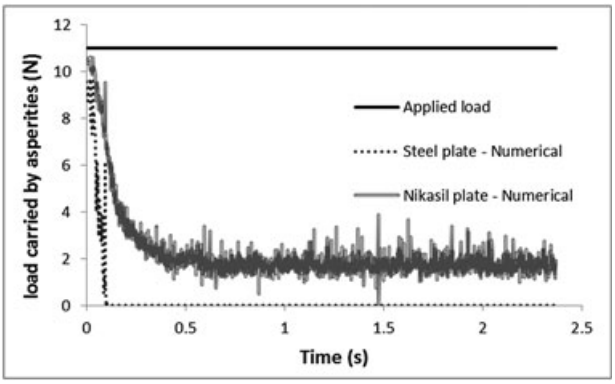


Figure 15. Predicted load share of asperities (boundary interaction).

Friction has not appreciably increased with the use of Ni-SiC with even rougher topographies than the parent steel substrate as demonstrated in Figure 16.

Referring to Figure 15, the analytical results indicate that the thin hydrodynamic film produced in the contact would be sufficient to keep the asperities of the smoother steel surfaces apart, whilst the same is not true for the case of the rougher Ni-Sic surface. This accounts for the observed prevalence of the mixed regime of lubrication. The relatively high coefficient of friction for the steel plate as shown in Figure 16 may indicate non-Newtonian shear of quite a thin film. An important aspect of this analysis is the validity of rather simple analytical method as opposed to the usual detailed and time consuming numerical analysis.

There are a number of implications for these findings. First, more defined topography with valleys and plateaus may be achieved with Ni-SiC than with the more ductile steel substrate. Surface modifications are usually carried out through cylindrical grinding/cross-hatch honing which is better suited to hard and brittle materials. With ductile materials, sharp features are difficult to produce and in many cases require further finishing operations in order to remove any excess ploughed residues. This means that for cross-hatch honed cylinder liners, Ni-SiC coating would be an advantage, which has been

© 2017 The Authors *Lubrication Science* Published by John Wiley & Sons Ltd.
DOI: 10.1002/ls

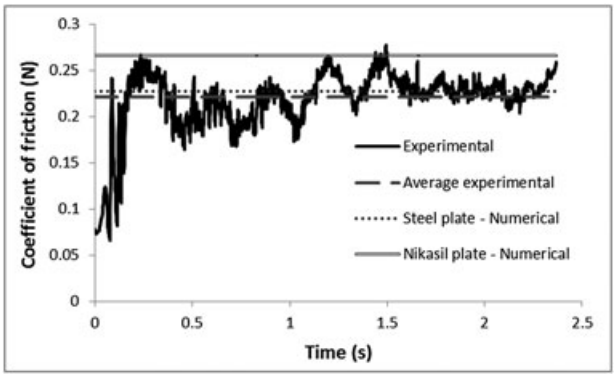


Figure 16. Coefficient of friction variation (experimental vs numerical).

shown by Howell-Smith.[42] Additionally, surface texturing of surfaces, particularly using laser ablation is being studied. Some preliminary work on this is reported either for partial dimpling of compression ring surface[43] or for chevron features on the cylinder liner surface in the vicinity of ring reversal[44] or on the surface of the piston skirt.[45] All these studies show some percentage gains in efficiency (reduced friction) due to hydrodynamic pressure perturbation of retained lubricant reservoirs. Again use of hard coatings lends itself to better controlled laser surface texturing. Second, with smoother surfaces, when boundary interactions occur, there would be a larger number of lower amplitude asperities, and as the boundary friction equation shows, this can be quite detrimental in terms of boundary friction.

CONCLUSIONS

The paper combines analytical and experimental investigation of sliding contact of a strip, with a representative profile to that of a piston top compression ring against a flat substrate with material choice, coating and topography, representative of a cylinder liner insert. The part of the 4-stroke engine cycle, at the TDC in transition from compression to the power stroke is investigated with representative of load intensity and sliding speed, using a precision fully instrumented designed sliding tribometer. The use of tribometer puts the focus of the investigation upon frictional performance of counter face geometry, topography and surface material. The approach eliminates the multi-variate multi-parameter nature of the problem, which occurs *in situ* in fired engines. The results clearly show the advantages and disadvantages of the highlighted parameters upon the regime of lubrication and the mechanisms underlying the generated friction.

ACKNOWLEDGEMENTS

The authors would like to express their gratitude to the Engineering and Physical Sciences Research Council (EPSRC) for the sponsorship of this research under the Encyclopaedic Program Grant (www.encyclopaedic.org). Thanks are also extended to the other partner organisations, particularly in this instance to Capricorn Automotive Ltd. for both its financial and technical support.

© 2017 The Authors *Lubrication Science* Published by John Wiley & Sons Ltd.
DOI: 10.1002/ls

REFERENCES

1. Richardson DE. Review of power cylinder friction for diesel engines. *Transactions of the ASME, Journal of Enggineering for Gas Turbines and Power* 2000; **122**:506–519.
2. Andersson P, Tamminen J, Sandstrom C-E. Piston ring tribology: a literature survey. *VTT Research notes* 2178, 2002, URL: http://www.inf.vtt.fi/pdf/
3. Tung SC, McMillan ML. Automotive tribology overview of current advances and challenges for the future. *Tribology International* 2004; **37**:517–536.
4. Fitzsimons B. Introduction to the importance of fuel efficiency and role of the encyclopaedic research project, in IMechE Seminar: A Drive for Fuel Efficiency, Loughborough 2011. 21 September 2011
5. Taylor CM. Fluid-film lubrication in the internal combustion engine: an invited review. *Journal of Physics D: Applied Physics* 1992; **25**:A91–A100.
6. Morris N, Rahmani R, Rahnejat H, King PD, Fitzsimons B. The influence of piston ring geometry and topography on friction. *Proceedings of the Institution of Mechanical Engineers, Part J: Journal of Engineering Tribology* 2013; **227** (2):141–153.
7. Bolander NW, Sadeghi F. Deterministic modeling of honed cylinder liner friction. *Tribology Transactions* 2007; **50**:248–556.
8. Spencer A, Almqvist A, Larsson R. A numerical model to investigate the effect of honing angle on the hydrodynamic lubrication between a combustion engine piston ring and cylinder liner. *Proceedings of the Institution of Mechanical Engineers, Part J: Journal of Engineering Tribology* 2011; **225**:683–689.
9. Tung SC, Huang Y. Modeling of abrasive wear in a piston ring and engine cylinder bore system. *Tribology Transactions* 2004; **47**:17–22.
10. Gore M, Perera M, Styles G, King PD, Rahnejat H. Wear characteristics of advanced honed and cross-hatched coated cylinder liners. *STLE 66th Annual Meeting & Exhibition*. Atlanta, Georgia, USA, May 15-19, 2011: p. 73
11. Styles G, Rahmani R, Rahnejat H, Fitzsimons B. In-cycle and life-time friction transience in piston ring–liner conjunction under mixed regime of lubrication. *International Journal of Engine Research* 2014; **15**(7):862–876.
12. Koch F, Fahl E, Haas A. A new technique for measuring the deformation of cylinder bores during engine operation. *SAE Paper No. 950540*, 1995.
13. Baker CE, Theodossiades S, Rahnejat H, Fitzsimons B. Influence of in-plane dynamics of thin compression rings on friction in internal combustion engines. *Journal of Engineering for Gas Turbines and Power* 2012; **134**(9):092801.
14. Mierbach A, Duck GE, Newman BA. Heat flow through piston rings and its influence on shape. *SAE Paper No. 831283*, 1983.
15. Harigaya Y, Suzuki M, Toda F, Takiguchi M. Analysis of oil film thickness and heat transfer on a piston ring of a diesel engine: effect of lubricant viscosity. *Journal of Engineering for Gas Turbines and Power* 2006; **128**(2006):685–693.
16. Morris N, Rahmani R, Rahnejat H, King PD, Fitzsimons B. Tribology of piston compression ring conjunction under transient thermal mixed regime of lubrication. *Tribology International* 2013; **59**:248–258.
17. Ma M-T, Sherrington I, Smith EH. Analysis of lubrication and friction for a complete piston-ring pack with an improved oil availability model - Part 2: circumferentially variable film. *Proceedings of the Institution of Mechanical Engineers, Part J: Journal of Engineering Tribology* 1997; **211**:17–27.
18. Mishra PC, Balakrishnan S, Rahnejat H. Tribology of compression ring-to-cylinder contact at reversal. *Proceedings of the Institution of Mechanical Engineers, Part J: Journal of Engineering Tribology* 2008; **222**(7):815–826.
19. Rahmani R, Theodossiades S, Rahnejat H, Fitzsimons B. Transient elastohydrodynamic lubrication of rough new or worn piston compression ring conjunction with an out-of-round cylinder bore. *Proceedings of the Institution of Mechanical Engineers, Part J: Journal of Engineering Tribology* 2012; **225**(4):284–305.
20. Shahmohamadi H, Rahmani R, Rahnejat H, Garner CP, King PD. Thermo-mixed hydrodynamics of piston compression ring conjunction. *Tribology Letters* 2013; **51**(3):323–340.
21. Arcoumanis C, Ostovar P, Mortier R. Mixed lubrication modelling of Newtonian and shear thinning liquids in a piston-ring configuration. *SAE Paper No. 972924*, 1997.
22. Sawicki JT, Yu B. Analytical solution of piston ring lubrication using mass conserving cavitation algorithm. *Tribology Transactions* 2000; **43**(3):419–426.
23. Shahmohamadi H, Mohammadpour M, Rahmani R, Rahnejat H, Garner CP, Howell-Smith S. On the boundary conditions in multi-phase flow through the piston ring-cylinder liner conjunction. *Tribology International* 2015; **90**:164–174.
24. Dearlove J, Cheng WK. Simultaneous piston ring friction and oil film thickness measurements in a reciprocating test rig. *SAE Paper No. 952470*, 1995.

© 2017 The Authors *Lubrication Science* Published by John Wiley & Sons Ltd.
DOI: 10.1002/ls

25. Ting LL. Development of a reciprocating test rig for tribological studies of piston engine moving components – part I: rig design and piston ring friction coefficients measuring method. *SAE Paper No. 930685*, 1993.
26. Akalin O, Newaz GM. Piston ring-cylinder bore friction modeling in mixed lubrication regime: part II – correlation with bench test data. *Transactions of the ASME, Journal of Tribology* 2001; **123**:219–223.
27. Bolander NW, Steenwyk BD, Kumar A, Sadeghi F. Film thickness and friction measurement of piston ring cylinder liner contact with corresponding modeling including mixed lubrication. *Proc. ICEF04, 2004 Fall Technical Conf. ASME Internal Combustion Engine Division*, Long Beach, California USA, Paper No. ICEF2004-903, October 24-27, 2004
28. Furuhama S, Sasaki S. New device for the measurement of piston frictional forces in small engines. *SAE technical paper*, No. 831284, 1983
29. Gore M, Theaker M, Howell-Smith S, Rahnejat H, King PD. Direct measurement of piston friction of internal combustion engines using the floating liner principle. *Proceedings of the Institution of Mechanical Engineers, Part D: Journal of Automobile Engineering* 2014; **228**(3):344–354.
30. Felter CL, Volund A, Imran T, Klit P. Development of a model capable of predicting the performance of piston ring–cylinder liner-like tribological interfaces. *Proceedings of the Institution of Mechanical Engineers, Part J: Journal of Engineering Tribology* 2010; **224**:877–883.
31. Johansson S, Nilsson PH, Ohlsson R, Rosen B-G. Experimental friction evaluation of cylinder liner/piston ring contact. *Wear* 2011; **271**:625–633.
32. Truhan JJ, Qu J, Blau PJ. A rig test to measure friction and wear of heavy duty diesel engine piston rings and cylinder liners using realistic lubricants. *Tribology International* 2004; **38**:211–218.
33. Morris N, Leighton M, De la Cruz M, Rahmani R, Rahnejat H, Howell-Smith S. Combined numerical and experimental investigation of the micro-hydrodynamics of chevron-based textured patterns influencing conjunctional friction of sliding contacts. *Proceedings of the Institution of Mechanical Engineers, Part J: Journal of Engineering Tribology* 2014; **229**(4):316–335.
34. Galligan J, Torrance AA, Liraut G. A scuffing test for piston ring/bore combinations: Pt. II. Formulated motor lubrication. *Wear* 1999; **236**:210–220.
35. Dellis P, Arcoumanis C. Cavitation development in the lubricant film of a reciprocating piston–ring assembly. *Proceedings of the Institution of Mechanical Engineers, Part J: Journal of Engineering Tribology* 2004; **218**:157–171.
36. Tung SC, Gao H. Tribological characteristics and surface interaction between piston ring coatings and a blend of energy-conserving oils and ethanol fuels. *Wear* 2003; **255**:1276–1285.
37. Howell-Smith S, Rahnejat H, King PD, Dowson D. Reducing in-cylinder parasitic losses through surface modification and coating. *Proceedings of the Institution of Mechanical Engineers, Part D: Journal of Automobile Engineering* 2014; **228**(4):391–402.
38. Gohar R, Rahnejat H. Fundamentals of Tribology. Imperial College Press, London 2008.
39. Greenwood JA, Tripp JH. The contact of two nominally rough surfaces. *Proceedings of the Institution of Mechanical Engineers, Part C: Journal of Mechanical Engineering Science* 1971; **185**:625–633.
40. Teodorescu M, Balakrishnan S, Rahnejat H. Integrated tribological analysis within a multi-physics approach to system dynamics. *Tribology and Interface Engineering Series (Elsevier)* 2005; **48**:725–737.
41. Dowson D. Elastohydrodynamic and micro-elastohydrodynamic lubrication. *Wear* 1995; **190**:125–138.
42. Howell-Smith SJ. Tribological optimisation of the internal combustion engine piston to bore conjunction through surface modification. *PhD Thesis*, *Loughborough University*, Loughborough, UK, 2011
43. Etsion I. Surface Texturing for in-Cylinder Friction Reduction. Woodhead Publishing Ltd, New Delhi (India) 2010.
44. Rahnejat H, Balakrishnan S, King PD, Howell-Smith S. In-cylinder friction reduction using a surface finish optimization technique. *Proceedings of the Institution of Mechanical Engineers, Part D: Journal of Automobile Engineering* 2006; **220**(9):1309–1318.
45. Balakrishnan S, Howell-Smith S, Rahnejat H. Investigation of reciprocating conformal contact of piston skirt-to-surface modified cylinder liner in high performance engines. *Proceedings of the Institution of Mechanical Engineers, Part C: Journal of Mechanical Engineering Science* 2005; **219**(11):1235–1247.
46. Naghieh GR, Rahnejat H, Jin ZM. Characteristics of frictionless contact of bonded elastic and viscoelastic layered solids. *Wear* 1999; **232**(2):243–249.
47. Johnson KL. Contact Mechanics. Cambridge Univ. Press, Cambridge 1985.

© 2017 The Authors *Lubrication Science* Published by John Wiley & Sons Ltd.
DOI: 10.1002/ls

APPENDIX

Under highly load conditions, localised deformation of contiguous surfaces can occur, and elastohydrodynamic regime of lubrication occurs. Any localised deformation may be approximated by a Hertzian contact, where[38]

$$\delta = \frac{F/L}{\pi E^*}\left\{1 + \ln\left[\frac{\pi E^* L^2}{2R(F/L)}\right]\right\} \tag{A1}$$

where, F is applied contact load, R and L are the strip (ring contacting radius of curvature) and contact length, respectively. The equivalent Young's modulus of elasticity for the contacting pair is

$$\frac{1}{E^*} = \frac{1-v_1^2}{E_1} + \frac{1-v_2^2}{E_2} \tag{A2}$$

This model represents a rigid ellipsoidal solid loaded against a semi-infinite elastic half-space of modulus E'. It should be noted that for coated solids, such as the cylinder liner and the compression ring, the ratio of the Hertzian footprint semi-half width to the thickness of the coatings (in each case): $\frac{a}{d} < 0.25$ indicates that the solid may be considered as a semi-infinite half-space and the underlying small strain classical Hertzian theory can be upheld.[46] Then, in the case of elastic line contact

$$a = \left(\frac{4FR}{\pi LE'}\right)^{1/2} \tag{A3}$$

when, $\frac{a}{d} \geq 2$, then the contacting surface is considered as a layered bonded solid and the classical Hertzian theory no longer applies, for which analytical expressions exist in some previous studies.[38,46,47] For the intervening period $0.25 > \frac{a}{d} \geq 2$, a numerical solution is required.

For the cases studies here, the strip is uncoated, thus is regarded as a semi-infinite solid and the flat specimen are either uncoated or furnished with a 20–50 μm thick coating of Ni-SiC. Using the data provided, $\frac{a}{d} << 0.25$ and thus: $\delta \approx 9\ nm$, which is inappreciable. Therefore, for all the tests reported in this paper contact conditions remain in the regions hydrodynamic, mixed and boundary regimes of lubrication.

© 2017 The Authors *Lubrication Science* Published by John Wiley & Sons Ltd.

DOI: 10.1002/ls